THE JOURNAL OF PHYSICAL CHEMISTRY C

Article

pubs.acs.org/JPCC

Controlled Preparation of Uniform TiO_2-Catalyzed Silver Nanoparticle Films for Surface-Enhanced Raman Scattering

Dawei Li, Lujun Pan,* Shuai Li, Kun Liu, Shifa Wu, and Wei Peng

School of Physics and Optoelectronic Technology, Dalian University of Technology, Dalian, Liaoning, 116024, People's Republic of China

ABSTRACT: Silver nanoparticle (AgNP) film is a kind of useful material in biochemical and biomedical fields as it can be used as a sensor based on its surface plasmon resonance for surface enhanced Raman scattering (SERS) analysis. In this work, a uniform AgNP film with controlled nanoparticle size, shape, and density have been prepared on TiO_2 film in a $AgNO_3$ solution by photocatalysis reduction method. The influences of TiO_2 film thickness and morphology on the AgNP's growth have been systemically studied. It is found that a thicker TiO_2 film with nanocrystalline morphology leads to a higher AgNP's growth rate, while a thinner TiO_2 film with membrane morphology leads to a lower AgNP's growth rate. Experimental SERS results show that the AgNP film prepared with different TiO_2 films and ultraviolet light irradiation time exhibit different SERS signals of rhodamine 6G (10^{-6} M). Atomic force microscope and scanning electron microscope analysis reveal that the size effect is a key factor affecting the SERS of our prepared AgNP films, which has also been evaluated by finite-difference time-domain simulation. It is found that the larger the average AgNP's size ($\leq\lambda/4$) and roughness, the higher the Raman enhancement. The SERS mapping images exhibit a good uniform Raman enhanced results in our prepared TiO_2-catalyzed AgNP film with a low relative standard deviation of approximately 10%.

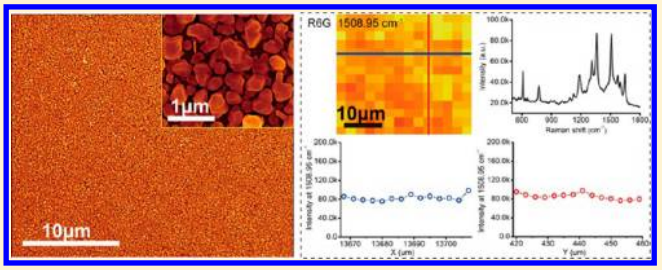

1. INTRODUCTION

Titanium dioxide (TiO_2) of anatase form is a wide band semiconductor with a band gap of 3.26 eV that can be excited under the irradiation of UV light with a wavelength less than 380 nm to produce electron−hole pairs.[1] These photogenerated electrons and holes can diffuse to the surface of TiO_2 to activate the photocatalytic reaction. Due to their excellent optical, photochemical, and antibacterial activities, nanoscaled TiO_2 particles have been widely used in many fields, such as self-cleaning,[2] photocatalysis,[3−5] and solar cells.[6−9] However, there still exist two main drawbacks for improving the photocatalytic activity of TiO_2, the low quantum yield and the lack of visible light activation, which are an obstacle to the overall applications.[10−12] It is considered that the low quantum yield is caused by the high rate of photogenerated electron−hole recombination; besides, TiO_2 has a quite wide band gap, allowing the exploitation of only 3−5% of all radiant solar energy.[13−15]

Noble metal nanoparticles such as Au and Ag have unique optical,[16] magnetic,[17] and catalytic properties.[18] Some research groups have experimentally proven that Ag nanoparticles (AgNPs) can act as electron traps aiding electron−hole separation.[19−21] In addition, AgNPs facilitate electron excitation by creating localized plasmon polaritons on AgNP surface, which causes a strong increase of local electric field (E-field) intensity. Therefore, combination of the two materials together, forming Ag−TiO_2 hybrids, would significantly enhance the photocatalytic reaction rate of TiO_2, exhibit more excellent properties, which would be applied in more fields. Kawahara et al. have found that Ag−TiO_2 nanocomposite films prepared by loading nanoporous TiO_2 films with AgNPs by photocatalytic reduction of Ag^+ ion exhibit multicolor photochromism.[22] This material with the unique property has the potential applications in cheap color rewritable papers and a new class of multiwavelength optical memories. Awazu et al. have prepared a plasmonic photocatalyst consisting of AgNPs embedded in TiO_2 and the measured photocatalytic activity under near UV irradiation of such photocatalyst, monitored by decomposition of methylene blue, was enhanced by a factor of 7.[14] It is expected that plasmonic photocatalysis would be of use as a high performance photocatalyst in nearly all current applications, particularly in locations of minimal light exposure. Similarly, Sung-Suh and Seery et al. have found significant enhancement in the Ag−TiO_2 photoactivity (such as photocatalytic degradation of rhodamine B and rhodamine 6G (R6G)), even under visible light irradiation, which can be ascribed to the increasing visible absorption capacity due to the presence of AgNPs.[23,24] Recently, the application of Ag−TiO_2 hybrids as a surface plasmon resonance (SPR) sensor has also been widely investigated.[25−29] It is a common knowledge that the signal enhancement of SPR sensor closely depends on the factors related to the nature of the AgNPs, such as their shape, size, interparticle spacing, as well as their dielectric environment. Therefore, the controlled design of Ag−TiO_2 composites

Received: January 23, 2013
Revised: March 14, 2013
Published: March 15, 2013

   dx.doi.org/10.1021/jp400778k | J. Phys. Chem. C 2013, 117, 6861−6871

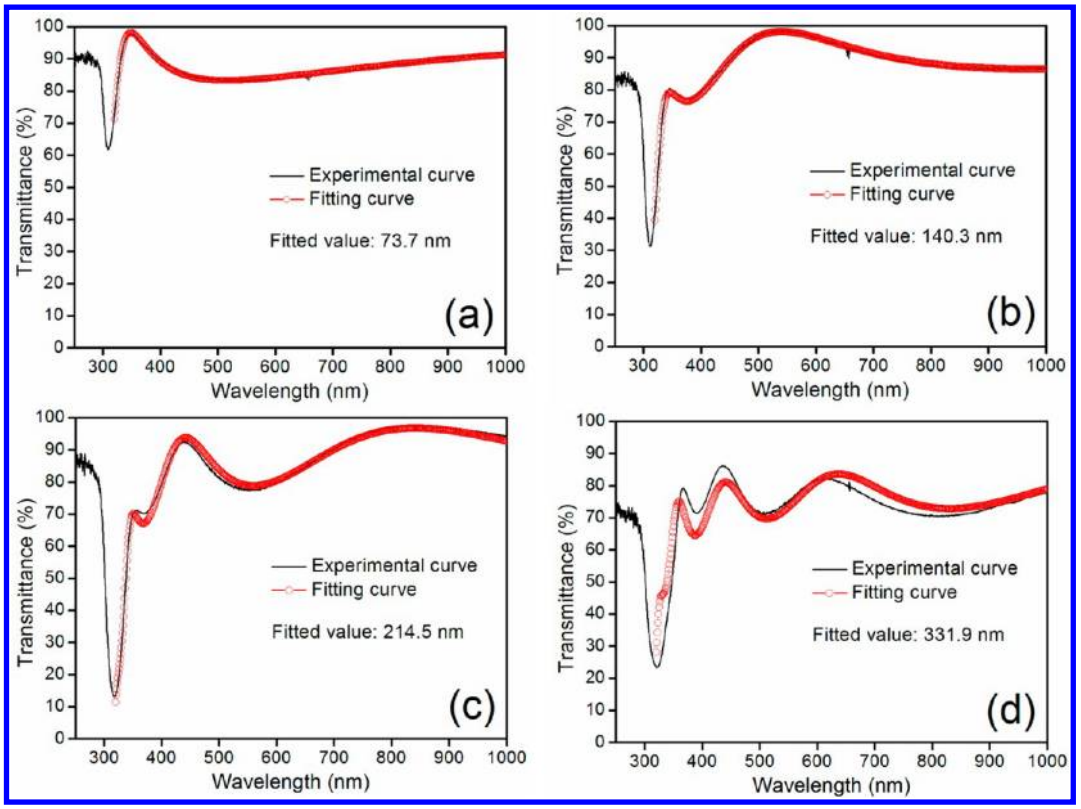

Figure 1. Optical transmission spectra of TiO_2 films with different thicknesses: (a) TiO_2(H1), (b) TiO_2(H2), (c) TiO_2(H3), and (d) TiO_2(H4).

is very meaningful and important for the above potential applications. From all reported methods for preparing Ag–TiO_2 nanoparticle-film hybrids, photocatalytic reduction is considered to be a simple and efficient one, where Ag^+ ion is reduced at the surface of the TiO_2 by photogenerated electrons.[1,22,25−33] In this method, the properties of TiO_2 film such as the morphology and crystal structure obviously affect the photocatalytic activity for the photocatalytic decomposition of aqueous acetic acid.[34] To our knowledge, the effect of TiO_2 film thickness and morphology on the growth of AgNPs during the photocatalysis reduction, and the corresponding surface enhanced Raman scattering (SERS) have not been known yet.

In this paper, a simple and versatile strategy for the controlled preparation of uniform AgNP films have been investigated, based on the photoreduction growth of AgNPs on TiO_2 film. The Raman enhancement of as-prepared TiO_2-catalyzed AgNP film has also been evaluated experimentally and theoretically, and the optimized TiO_2-catalyzed AgNP film exhibit a highly sensitive SERS activity. This work is valuable in controlled designing TiO_2-catalyzed AgNP film used as a SERS-active sensor.

2. EXPERIMENTAL SECTION

2.1. Preparation of TiO_2 Film. TiO_2 film was prepared by an ordinary sol–gel method. A total of 50 mL of tetrabutyl orthotitanate and 3 mL of acetylacetone were mixed and stirred for 10 min (called solution A); meanwhile, 110 mL of alcohol, 1.4 mL of deionized water, and 0.2 mL of nitric acid were mixed and stirred for 10 min (called solution B). Then solution B was dropwise added into solution A during the stirring process, and the mixture solution was stirred for 30 min, forming the TiO_2 sol solution. TiO_2 film was deposited onto the glass substrate by a dip-coating method, and the thickness of TiO_2 film was controlled by adjusting the lifting rate from 50 to 300 mm/min. At last, the sample was calcined at 450 °C for 1 h in order to crystallize and form the anatase phase TiO_2 film.

2.2. Growth of AgNPs on TiO_2 Films. The growth of AgNPs on TiO_2 films was carried out in a dark room. The TiO_2-coated glass substrate were irradiated with the UV light (wavelength: 253 nm) from a low pressure mercury lamp (power: 6 W) in a 3 mM $AgNO_3$ solution to photocatalytically deposit AgNPs, where the distance between the substrate and the UV lamp was approximately 6 cm. The whole AgNP's growth process was monitored with a UV–visible spectrometer, and the spectra were recorded per minute. After irradiation, the substrates were removed from $AgNO_3$ solution, dried in air, and stored in the dark room.

2.3. SERS Measurement. R6G with a concentration of 10^{-6} M was selected as the probe molecules. The above samples were soaked in the R6G solution for 1 h. Then the samples with R6G molecules were taken out and washed with deionized water to remove the free molecules and dried in air. At last, Raman spectra were measured under the same conditions as follows: a 632.8 nm He–Ne laser with a power of 3.28 mW was used as the exciting light; a 50× objective was used to focus the laser beam onto the sample surface and to collect the Raman signal; the size of the laser spot was about 2 μm; and the spectra were recorded with an accumulation time of 10 s. The measurement of Raman spectra for each sample was repeated five times.

2.4. Characterization. The products were studied and analyzed by UV–visible spectrometer (Ocean Maya2000-Pro, U.S.A.), atomic force microscope (AFM; Agilent PicoPlus II, Agilent, Santa Clara, CA), scanning electron microscope (SEM, Nova NanoSEM 450, FEI), and Raman spectrometer (Renishaw inVia plus, Renishaw, Gloucestershire, U.K.).

dx.doi.org/10.1021/jp400778k | J. Phys. Chem. C 2013, 117, 6861−6871

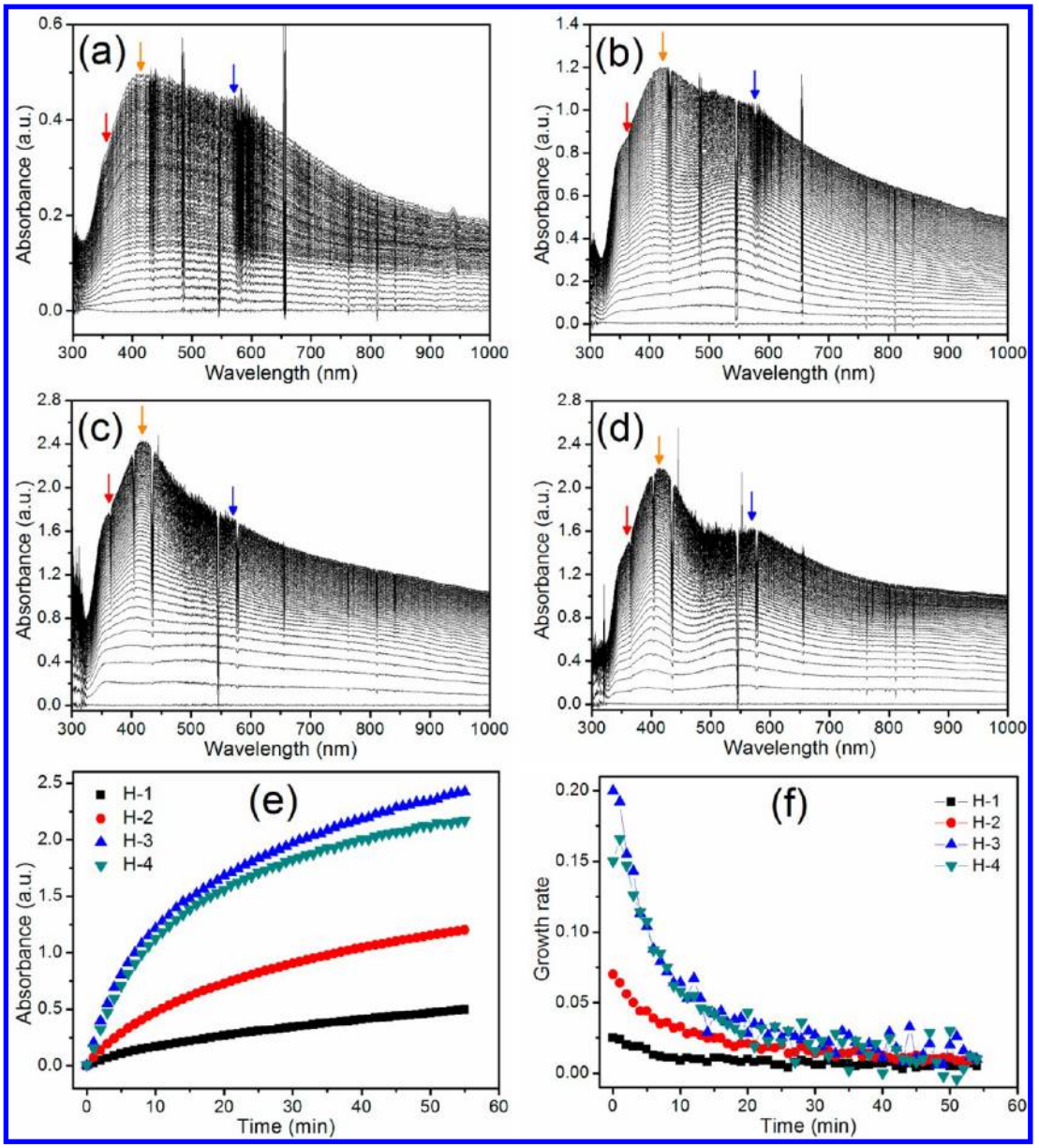

Figure 2. In situ and real-time UV−visible absorption spectra of AgNPs grown on (a) TiO_2(H1), (b) TiO_2(H2), (c) TiO_2(H3), and (d) TiO_2(H4) in 3 mM $AgNO_3$ solution with UV irradiation for 60 min. Time dependence of (e) absorbance maximum and (f) growth rate of AgNPs on TiO_2 films with different film thicknesses.

3. RESULTS AND DISCUSSION

Figure 1 shows the optical transmission spectra of TiO_2 films with four different thicknesses deposited on the glass substrates. All the spectra are measured in the wavelength range from 200 to 1000 nm. In each spectrum, there exist two curves in each figure. The continuous line represents experimental data and the hollow circle line is the corresponding fitting curve by envelop method.[35] The periodic oscillations observed in the spectra are due to interferences between reflections at the air−TiO_2 and the TiO_2−glass interfaces. The absorption edges of each TiO_2 film are observed around 300 nm. The thicknesses of the TiO_2 films in Figure 1a−d can be measured using the above fitting method, which are calculated to be approximately 74, 140, 214, and 330 nm, respectively. For convenience, the samples are labeled as TiO_2(H1), TiO_2(H2), TiO_2(H3), and TiO_2(H4), corresponding to the TiO_2 films with thicknesses of 74, 140, 214, and 330 nm, respectively. It is found that the transmission rate decreases with the increase of TiO_2 film thickness and the maximum transmission varies from 98 to 86%.

Figure 2a−d show the in situ and real-time UV−visible absorption spectra of AgNPs grown on TiO_2 films with different thicknesses in 3 mM $AgNO_3$ solution under the UV irradiation for 60 min. In each spectrum, it is clearly observed that, at the beginning of the UV irradiation, a broad absorbance band containing three absorption peaks (indicated by arrows) appear in the spectra. The positions of these three peaks are at approximately 360 (weak), 420 (strong), and 570 nm (medium), which correspond to the AgNP's out-of-plane quadrupole resonance, out-of-plane dipole resonance, and in-plane quadrupole resonance, respectively.[36] With continuous increasing of UV irradiation time, the absorption intensity for the AgNPs gradually increases, indicating that more and more AgNPs are grown on the TiO_2 film surface. It is considered that

dx.doi.org/10.1021/jp400778k | J. Phys. Chem. C 2013, 117, 6861−6871

there is a linear relation between the absorbance of AgNPs on TiO_2 film and the amount of AgNPs grown on TiO_2 film. Therefore, to assess the effect of TiO_2 film thickness on the growth of AgNPs, we have compared the time dependence of absorbance maximum (the strong peak at approximately 420 nm) and the growth rate of AgNPs on TiO_2 film with thickness from 74 to 330 nm, as shown in Figures 2e and 2f. The growth rate of AgNPs shown in Figure 2f is defined as the rate of absorbance maximum vs irradiation time, which is obtained by derivative calculation for the data of absorbance maximum vs irradiation time shown in Figure 2e. It is found that the growth rate of AgNPs is obviously increased with the TiO_2 film thickness from 74 to 214 nm, but no longer increased when the TiO_2 film thickness reaches up to 330 nm.

Why does the TiO_2 film thickness affect the growth rate of AgNPs so greatly? So far, the mechanism for this phenomenon is not well-known yet, but one thing is sure: the growth rate of AgNPs is directly determined by the photocatalytic activity of TiO_2 film. The higher the activity of TiO_2 film, the faster the growth rate of AgNPs. The main possible reason for the above phenomenon could be explained as follows. When the TiO_2 film thickness is lower than a certain thickness, the TiO_2 cannot totally absorb the UV light whose energy is higher than the TiO_2 band gap energy. As the TiO_2 film thickness increases, the absorption of UV light increases, then the production rate of photogenerated electron−hole pairs increases. However, when the thickness of TiO_2 film increases to a level that can absorb the UV light totally, the production rate of photogenerated electron−hole pairs is no longer increased, even if the film thickness is continually increased. The above idea of complete UV light absorption is well supported by the TiO_2 transmission curves shown in Figure 1. In our experiment, the total absorption of UV light by TiO_2 film with a thickness of 330 nm has been saturated, and then the amount of photogenerated electron−hole pairs is no longer increased. On the other hand, to realize the reaction of the photogenerated electrons with Ag^+ ion, the diffusion process of generated electron−hole pairs in the TiO_2 to the surface is needed. It is noted that the diffusion length of the photocarriers (electron−hole pairs) is an order of nanometers.[37] For thinner TiO_2 film, with increasing of the TiO_2 film thickness, more electrons per unit time can diffuse to the surface and react with Ag^+ ions; when the thickness of TiO_2 film reaches or exceeds a certain level, some of the photocarriers annihilate because of the recombination before arriving at the TiO_2 surface. Therefore, TiO_2 film thickness has a saturation value for the photocatalytic reaction due to the saturation of light-harvesting efficiency and the changes in electron transport.[37,38]

Figure 3 compares the AFM morphological images of AgNPs deposited on TiO_2 films with different thicknesses (vertical comparison) after UV irradiation in 3 mM $AgNO_3$ solution for 2−60 min (horizontal comparison). The changes of AgNPs grown on the TiO_2(H1)-film for different UV irradiation time are shown in Figure 3A1−A5. It is observed that the UV irradiation on TiO_2(H1)-film leads to the self-organized AgNPs with a high density and the NP size largely depends on the UV irradiation time. After a 2 min UV irradiation, sparsely distributed very small AgNPs (bright spots) with sizes down to a few nanometers are observed from the AFM image (Figure 3A1). After 8 min irradiation, the surface of TiO_2(H1)-film has almost been covered with small spherical AgNPs with a narrow dispersion in particle size, typically with a diameter of (36.0 ± 4.6) nm (Figure 3A2). Further irradiation appears to increase

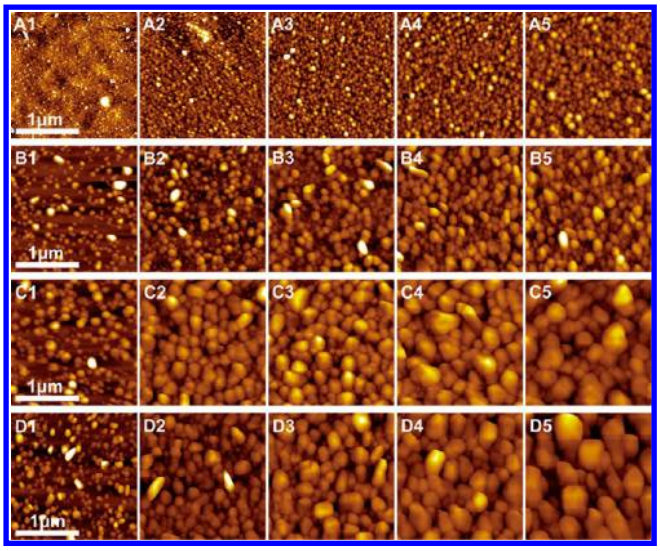

Figure 3. (A1−A5) AFM images of AgNPs deposited on TiO_2(H1)-film in 3 mM $AgNO_3$ solution after UV irradiation for 2, 8, 16, 30, and 60 min. (B1−B5), (C1−C5), and (D1−D5) show the corresponding AFM images of AgNPs deposited on TiO_2(H2)-, TiO_2(H3)-, and TiO_2(H4)-films, respectively, with UV irradiation for 2, 8, 16, 30, and 60 min.

the size and density of AgNPs (Figure 3A3−A5). The similar growth rules of AgNPs have also been observed for the other three kinds of TiO_2 films with different thicknesses (horizontal comparison). There are more results and rules that could be obtained on close examination of the whole AFM images in Figure 3 as follows:

1. Under the same UV irradiation time, the average sizes of AgNPs grown on TiO_2 films with different thicknesses are increased in the order of AgNPs-TiO_2(H1) < AgNPs-TiO_2(H2) < AgNPs-TiO_2(H3) ≈ AgNPs-TiO_2(H4) (vertical comparison), which is consistent with the results of absorption spectral analysis. In addition, AgNPs grown on TiO_2(H2/H3/H4)-films possess different shapes, most of which are polygonal, differing from those grown on TiO_2(H1)-film.
2. A careful observation of Figure 3B illustrates that, after 2 min UV irradiation, only 50% of TiO_2(H2)-film surface is covered with AgNPs, indicating a higher AgNP growth rate in these areas (Figure 3B1). As the irradiation time is increased to 8 min, most of the TiO_2(H2)-film surface has been covered with AgNPs. However, the NP size distribution is wide (Figure 3B2). The difference in NP size distribution does not change a lot with further UV irradiation (Figure 3B3−B5).
3. Compared with NP size distribution in Figure 3B, the sizes of AgNPs grown on TiO_2(H3/H4)-films become relatively uniform (Figure 3C,D).
4. The root-mean-square (RMS) roughness of samples is obtained from the AFM images in Figure 3 (shown in Figure 4). The surface roughness is observed to be gradually increased within 60 min UV irradiation from (1.8 ± 0.4) to (49.9 ± 15.5) nm for TiO_2(H1), from (38.3 ± 15.7) to (101.1 ± 30.2) nm for TiO_2(H2), from (61.8 ± 22.3) to (162.6 ± 51.5) nm for TiO_2(H3), and from (50.7 ± 20.3) to (228.6 ± 76.8) nm for TiO_2(H4). This result is also in good agreement with that from the absorption spectral analysis.

dx.doi.org/10.1021/jp400778k | J. Phys. Chem. C 2013, 117, 6861−6871

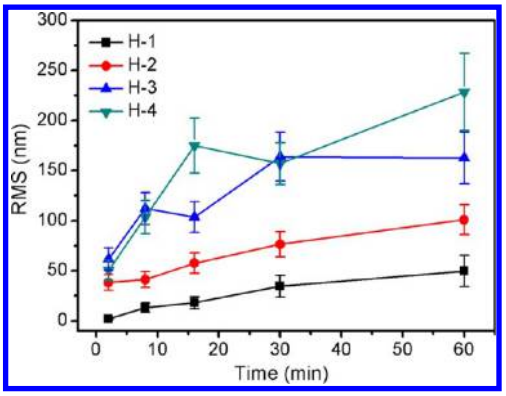

Figure 4. Time dependence of surface roughness for AgNP film with different TiO_2 film thickness.

At the same time, a question is raised that what leads to the different AgNP size distributions on these TiO_2 films with different thicknesses. According to the above UV−visible absorption and AFM analysis, TiO_2 film thickness only affects the photocatalytic growth rate of AgNPs, which is not considered to be the main factor that affects the NP size distribution. Kato et al. have reported that the morphology of TiO_2 films, such as pore size and pore distribution, obviously affects the photocatalytic activity for the photocatalytic decomposition of aqueous acetic acid.[34] To investigate the main causes of this phenomenon, AFM images of TiO_2 films with different thickness before irradiation have been compared, as shown in Figure 5. It is clearly observed from Figure 5a that the TiO_2(H1) film (74 nm) has a continuous membrane structure and flat texture with RMS roughness of approximately (1.6 ± 0.5) nm, which is similar to that observed in Figure 3A1. As the film thickness is increased to 140 nm, the surface appearance of TiO_2 changes dramatically (Figure 5b). Nearly half of the area has been covered with small TiO_2 NPs, typically (16.4 ± 0.6) nm in diameter, and the remaining area is still smooth in texture. With the further increasing of TiO_2 film thickness, the quantity and density of TiO_2 NPs continue to increase, but the sizes of TiO_2 NPs have changed very little (Figure 5c). As the TiO_2 film thickness reaches up to 330 nm, almost the entire film surface has been covered by closely packed, continuous TiO_2 NPs (Figure 5d). The variation of surface roughness with TiO_2 film thickness shown in Figure 5e also follows the above changing pattern of surface morphology. It is observed from the above AFM analysis that TiO_2 film contains two kinds of surface structures, namely, continuous membrane structure and granular texture. Raman analysis (shown in Figure 5f) indicates that the formed TiO_2 NPs are nanocrystalline, which is predominately in anatase phase, while the continuous membrane structure mainly corresponds to the amorphous phase of TiO_2. It is well-known that the photocatalytic activity is higher for TiO_2 in anatase phase than that in TiO_2 amorphous phase. Therefore, the different crystal structure distributions on the TiO_2 film are considered to be the key factor that affects the photocatalytic activity on the TiO_2 surface, which then leads to the growth of AgNPs with different size distributions under UV irradiation (Figure 3B).

Based on the experimental results and the above inferences, a possible model for the AgNP growth on the TiO_2 films with different thicknesses and morphologies is proposed, as shown in Figure 6. At the first step, TiO_2 films with different thicknesses (together with different crystal structures) are formed after calcination. The processes leading to the selective formation of the resulting AgNPs which absorb UV light begin from the second step. Under the UV irradiation, photogenerated electrons reduce Ag^+ ions to grow Ag nuclei. Simultaneously, new AgNPs seed at new sites on the TiO_2 film substrate. From TiO_2 film surfaces entirely covered by membrane structure (Figure 6a) or nanocrystalline structure

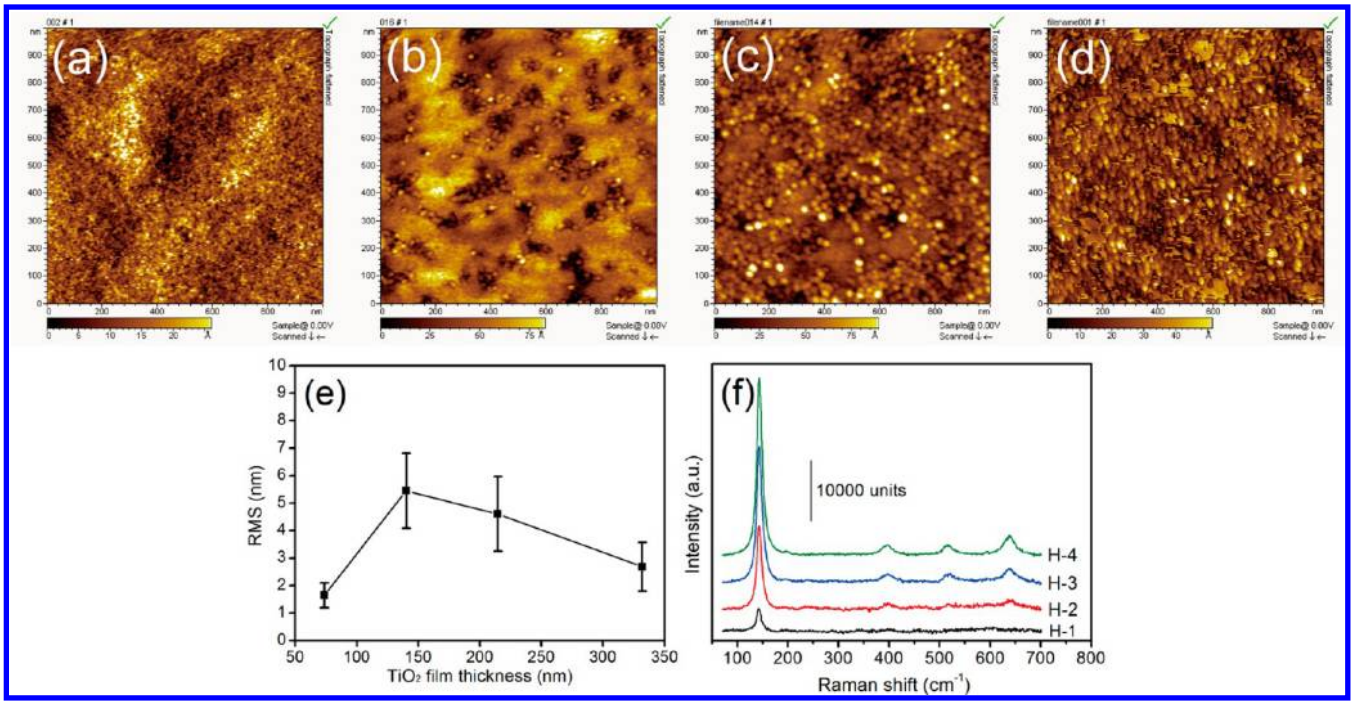

Figure 5. AFM images of (a) TiO_2(H1), (b) TiO_2(H2), (c) TiO_2(H3), and (d) TiO_2(H4) films that have been calcined at 450 °C for 60 min. (e) The variation of surface roughness with TiO_2 film thickness. (f) Raman spectra of TiO_2 films with different thicknesses.

dx.doi.org/10.1021/jp400778k | J. Phys. Chem. C 2013, 117, 6861−6871

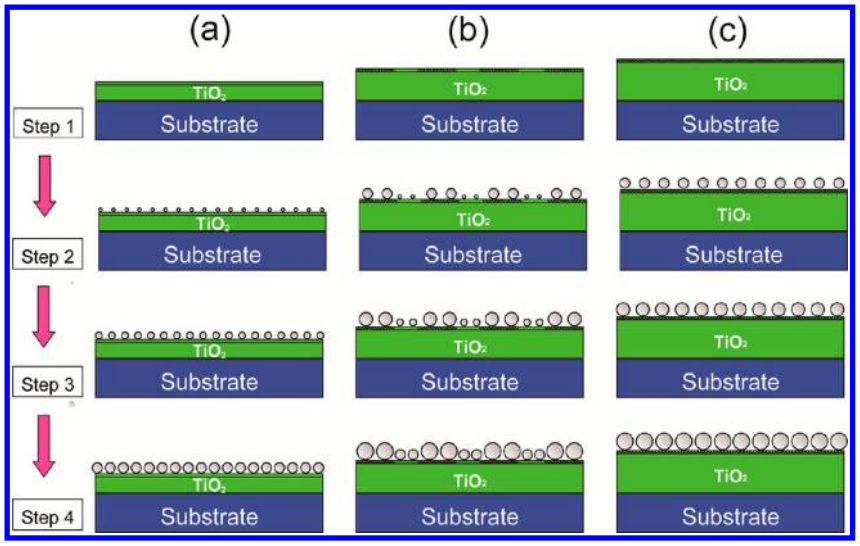

Figure 6. Proposed mechanism for growth of AgNPs on TiO_2 films with different film thicknesses and morphologies.

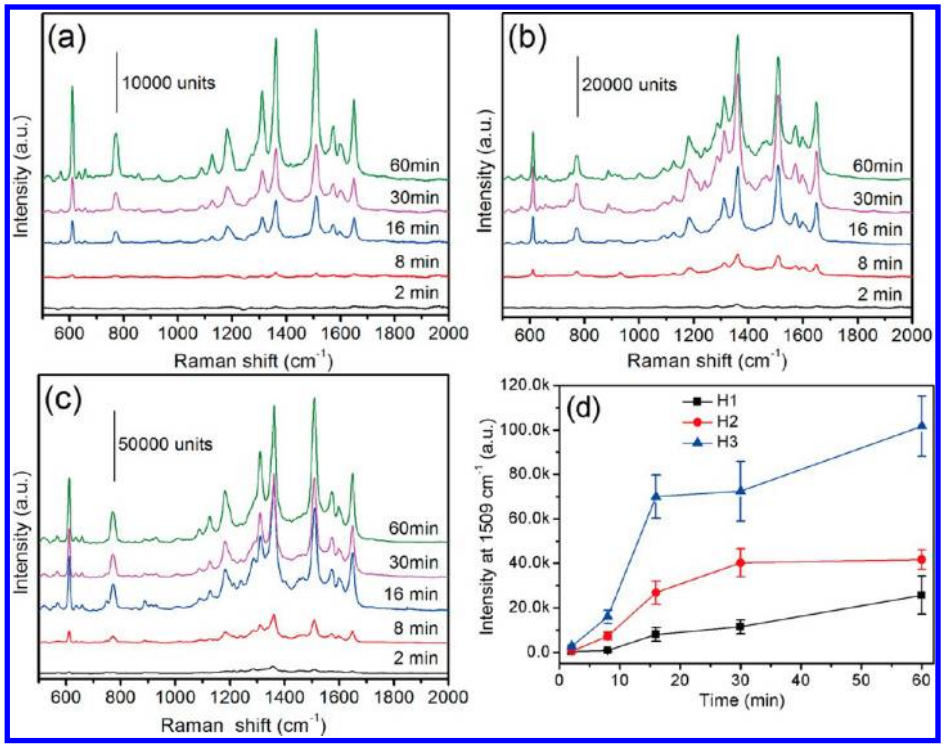

Figure 7. SERS spectra of R6G(10^{-6} M) on AgNP film (a) TiO_2(H1)-catalyzed, (b) TiO_2(H2)-catalyzed, and (c) TiO_2(H3)-catalyzed. (d) The dependence of SERS intensity at 1509 cm^{-1} on the TiO_2 film thickness and UV irradiation time.

(Figure 6c), the uniform AgNPs are likely to be grown; while from TiO_2 film surface with mixed heterogeneous structures (Figure 6b), AgNPs with different sizes are obtained. In addition, the sizes and distribution density of AgNPs can be efficiently controlled by adjusting film thickness and UV irradiation time.

So far, various SERS substrates or SPR sensors have been fabricated by using electron beam lithography, nanoimprint lithography, template assembly of NPs, spin-coating method, and so on.[39−43] In these methods, template self-assembly is employed utilizing the chemical interaction between NPs and the surface of substrates, which may introduce additional information during the SERS measurement. For the lithography, though it can produce an ordered pattern and can control the density of NP distribution; however, this method is complicated and expensive. In contrast, the photocatalytic method of producing AgNP film is process controllable, simple in operation and easy to be scaled up for industrial production. In addition, the deposited AgNPs on TiO_2 film are not easily to be washed off by deionized water or ethanol and so on. Prompted by these positive features, the factors that affect the SERS activity of our prepared TiO_2-catalyzed AgNP film is discussed as follows.

Figure 7a−c illustrates the average SERS spectra of R6G with a concentration of 10^{-6} M obtained from TiO_2-catalyzed AgNP films prepared under different UV irradiation time. As indicated by the results, in each figure, the signal intensity of SERS spectra increases proportionally with increasing of the UV

dx.doi.org/10.1021/jp400778k | J. Phys. Chem. C 2013, 117, 6861−6871

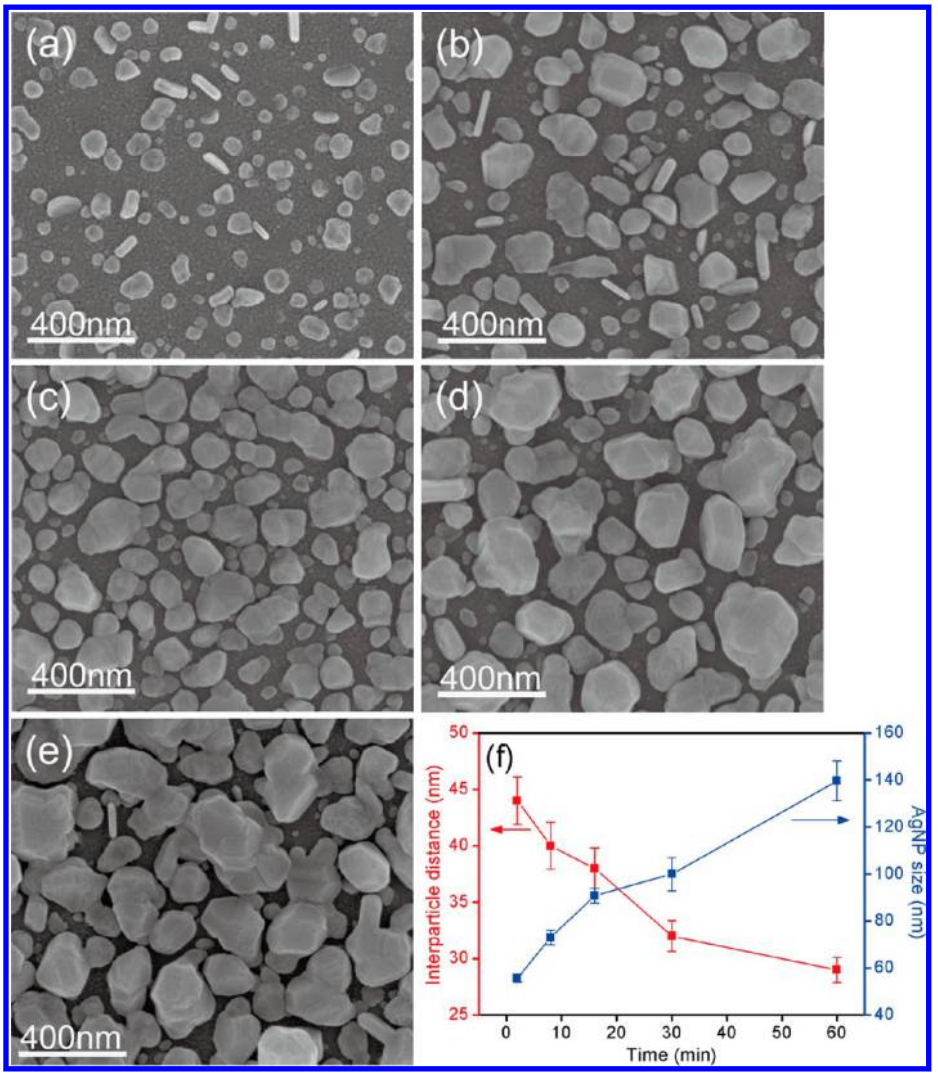

Figure 8. SEM images of AgNPs deposited on TiO_2(H3)-film after UV irradiation in 3 mM $AgNO_3$ solution for (a) 2, (b) 8, (c) 16, (d) 30, and (e) 60 min. (f) The variation of AgNP size and interparticle spacing with irradiation time.

irradiation time. To investigate and optimize the SERS activity of TiO_2-catalyzed AgNP film, curves of the SERS signal intensities at 1509 cm^{-1} as a function of film thickness under different UV irradiation times are plotted and compared, as shown in Figure 7d. Overall, the SERS activities of TiO_2-catalyzed AgNP film increase in the order of TiO_2(H1) < TiO_2(H2) < TiO_2(H3). A careful observation of Figure 7d shows that the dependence of SERS intensity on UV irradiation time is different for TiO_2 films with different thicknesses. For TiO_2(H1), the relation between SERS intensity and UV irradiation time is approximately linear; for TiO_2(H2), this relation curve is initially linear and gradually becomes saturated; while for TiO_2(H3), the relation curve rises quickly during the early reaction stage, then becomes saturated, and finally rises again. The question is what leads to such large differences in SERS activity among these TiO_2-catalyzed AgNP films. There are two mechanisms for SERS, namely, the electromagnetic enhancement due to the localized SPR mode and the chemical enhancement that arises from the interaction between molecules and NPs. In this report, R6G is selected because of its high binding affinity to silver surface. Therefore, the difference in the affinity or the number of probed R6G molecules in the Raman measurement can be ruled out. Then, the electromagnetic mechanism is considered to contribute most of the enhancement. It is also known that the electromagnetic enhancement strongly depends on the detailed physical structure of metal NPs such as their size, shape, and composition, interparticle spacing, and NP density. According to the above UV−visible absorption and AFM analysis, the difference in NP size may be one of the main factors that affect the SERS difference. However, whether interparticle spacing affects the SERS greatly is difficult to judge through AFM image due to the radius of the AFM probe tips, which lead to the broadening of the image and sequentially underestimating of interparticle spacing.

To further investigate the main causes of SERS difference, as an example, SEM images of AgNPs grown on TiO_2(H3)-film under different UV irradiation times have been compared (shown in Figure 8).

Consistent with the AFM images of Figure 3c, as the irradiation time increases, the AgNPs grow and coalesce rapidly, forming large NPs with irregular polyhedron structures. After 2 min UV irradiation, the size of NPs is approximately (55.6 ± 1.7) nm; while after 60 min, the NP size has reached up to (139.7 ± 8.4) nm. However, the average interparticle spacing has not changed too much, gradually decreased from

dx.doi.org/10.1021/jp400778k | J. Phys. Chem. C 2013, 117, 6861−6871

(44.2 ± 2.1) nm (2 min) to (29.3 ± 1.1) nm (60 min). The similar variations are also obtained for TiO_2(H1)-film and TiO_2(H2)-film (not shown here). Figure 9 illustrates the

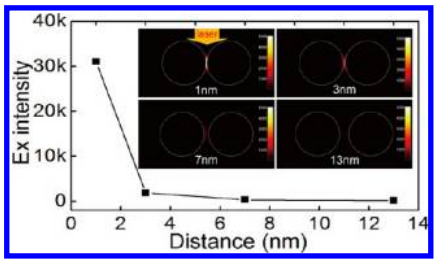

Figure 9. FDTD simulation of E-field distribution at the gap between two adjacent AgNPs with an interspacing ranging from 1 to 13 nm. Laser wavelength: 632.8 nm. The diameter of the AgNP: 60 nm.

calculated E-field distribution between two adjacent AgNPs by using finite-difference time-domain (FDTD) simulation. It can be seen from the inset of Figure 9 that the localized surface plasmon can be excited in the nanogaps between AgNPs (so-called hot spots), producing a strong E-field enhancement and subsequently a great increase of the Raman intensity for molecules absorbed on the NP surface. However, the E-field intensity (SERS signal) decreases exponentially with increasing the spacing of NPs. When the spacing is larger than 10 nm, the coupling interaction between AgNPs is very weak and can be ignored. In our system, the interparticle spacing is much larger than 10 nm, therefore, the NP size effect is considered to play the major role in SERS enhancement. To further confirm this effect, we have plotted the dependence of SERS intensity at 1509 cm^{-1} on the average AgNP size, obtained from the plot of particle size versus growth time (Figure 8f) and the plot of SERS intensity versus growth time (Figure 7d), as shown in Figure 10. It is found that the intensities of the observed SERS

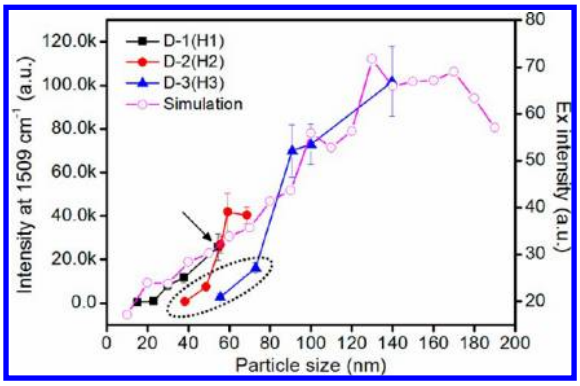

Figure 10. The dependence of SERS intensity at 1509 cm^{-1} on the average AgNP size.

signal increase with the increase of the AgNP sizes. It is noted that the data for TiO_2(H1) and TiO_2(H2) overlap at the same particle size of 55 nm indicated by the arrow, suggesting a distinct size effect. The curve with hollow dots in Figure 10 illustrates the FDTD simulation result (excitation wavelength: 632.8 nm), showing that the E-field intensity (SERS signal) first increases gradually with the increasing of the NP size, and then it reaches a maximum when the NP size is approximately 130 nm. However, the further increase in the NP size results in a slow (from 130 to 160 nm) and then a rapid (larger than 170 nm) decrease in the E-field intensity. This tendency is almost the same as that for the dependence of E-field intensity on Au NP size reported by Tian et al.[44] The appearance of maximum at wavelength of 130 nm ($\leq\lambda/4$) is considered to be due to the surface plasmon resonance of NP under the excitation of the probe laser. In addition, it is observed that the simulation result is in good agreement with the experimental data, which is a further proof that the size effect plays a main role in the SERS enhancement. However, some data do not fall in the calculated curve, shown by the dotted line circle, which is observed to be lower in SERS intensity than the others with the similar NP sizes. The main reason for this phenomenon is considered to be the difference in NP distribution density.

Both SERS substrate and SPR sensor should have the features of high signal enhancement, good reproducibility and uniformly surface roughness etc. to realize their commercial applications. To evaluate these performances of our prepared TiO_2-catalyzed AgNP film, a Raman mapping of R6G with low concentration on the TiO_2-catalyzed AgNP film has been made. Figure 11a and b show the low magnified optical microscopic and SEM images of TiO_2(H3)-catalyzed AgNP film after UV irradiation for 60 min. It is observed that one layer of AgNPs is formed, and AgNPs distribute densely and uniformly on the whole substrate, which would be suitable for quantitative or semiquantitative analysis. The Raman mapping of R6G with a concentration of 10^{-6} M on the TiO_2(H3)-catalyzed AgNP film is shown in Figure 11c. The top left in this figure illustrates the measured region and the brightness is proportional to the R6G signal intensity at 1508.95 cm^{-1}; the top right is a typical Raman spectral of the measured area; the bottom left and right in (c) are the corresponding sectional views of the two crossed lines shown in the figure of top left. The relatively strong signal of R6G with low concentration can be detected, indicating that this TiO_2(H3)-catalyzed AgNP film has a high SERS activity. The standard deviation in SERS enhancement σ (probed at different locations for the single film) for the TiO_2(H3)-catalyzed AgNP film is estimated as follows:

$$\sigma = \frac{1}{\bar{I}}\sqrt{\frac{1}{N}\sum_{i=1}^{N}(I_i-\bar{I})^2} \times 100\% \quad (1)$$

and

$$\bar{I} = \frac{1}{N}\sum_{i=1}^{N} I_i \quad (2)$$

where N is the number of SERS spectra of R6G (10^{-6} M), which are measured at different locations on the same film, I_i is the R6G signal intensity at 1508.95 cm^{-1} detected at the ith location, and $\bar{I}$ is the average R6G signal intensity. Herein, a total of 196 (14 × 14) SERS spectra of R6G have been measured. According to eqs 1 and 2, we get $\sigma \approx 10\%$. Such low spot-to-spot variance reveals that the AgNP film prepared by photocatalysis reduction method can be used as a uniform and reproducible SERS active substrate.

4. CONCLUSIONS

A simple and versatile method for the growth of uniform AgNP film, based on the photoreduction growth of AgNPs on TiO_2 film, has been studied. The morphology and the factors that affect SERS activity of the AgNP films prepared under different conditions have been compared. It is found that the TiO_2 film thickness and morphology greatly affect the size distribution and density of the grown AgNPs. The Raman enhancement of

dx.doi.org/10.1021/jp400778k | J. Phys. Chem. C 2013, 117, 6861−6871

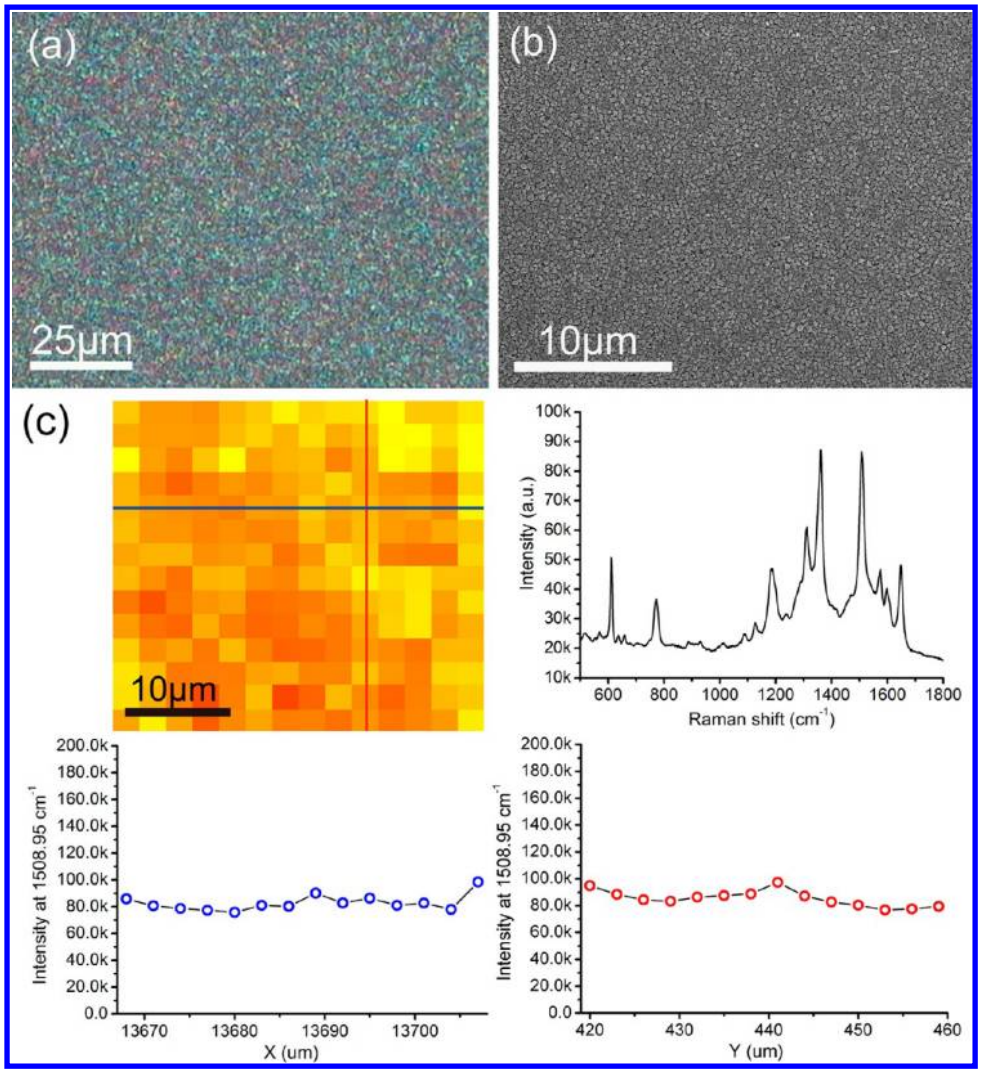

Figure 11. (a) Optical microscopic and (b) SEM images of TiO_2(H3)-catalyzed AgNP film after UV irradiation for 60 min. (c) SERS mapping (step size: 3 μm, mapping area: 14 × 14 = 196 points) of R6G with a concentration of 10^{-6} M on TiO_2(H3)-catalyzed AgNP film after irradiation for 60 min. The top left in (c) illustrates the measured rectangular region and the brightness is proportional to the R6G signal intensity at 1508.95 cm^{-1}, the top right in (c) is the spectral line of the intersection, the bottom left and right in (c) are the corresponding sectional views of the two crossed lines.

the as-prepared AgNP film has also been evaluated experimentally and theoretically, and the optimized AgNP film exhibits a highly sensitive SERS activity. The low film to film variance (≈10%) suggests that the AgNP films prepared by the photocatalysis method have the potential to be used as a uniform and reproducible SERS sensor for quantitative or semiquantitative analysis.

AUTHOR INFORMATION

Corresponding Author

*Tel.: +86-411-84707863-334. Fax: +86-411-84709304. E-mail: lpan@dlut.edu.cn.

Notes

The authors declare no competing financial interest.

ACKNOWLEDGMENTS

This work was supported by the National Natural Science Foundation of China (Nos. 11074029, 61137005, and 11274055) and the Fundamental Research Funds for the Central Universities (No. DUT12ZD204).

REFERENCES

(1) Ahmed, M. H.; Keyes, T. E.; Byrne, J. A.; Blackledge, C. W.; Hamilton, J. W. Adsorption and Photocatalytic Degradation of Human Serum Albumin on TiO_2 and Ag−TiO_2 Films. *J. Photochem. Photobiol., A* **2011**, *222* (1), 123−131.

(2) Andersson, M.; Österlund, L.; Ljungström, S.; Palmqvist, A. Preparation of Nanosize Anatase and Rutile TiO_2 by Hydrothermal Treatment of Microemulsions and Their Activity for Photocatalytic Wet Oxidation of Phenol. *J. Phys. Chem. B* **2002**, *106* (41), 10674−10679.

(3) Hoffmann, M. R.; Martin, S. T.; Choi, W.; Bahnemann, D. W. Environmental Applications of Semiconductor Photocatalysis. *Chem. Rev.* **1995**, *95* (1), 69−96.

(4) Jagadale, T. C.; Takale, S. P.; Sonawane, R. S.; Joshi, H. M.; Patil, S. I.; Kale, B. B.; Ogale, S. B. N-Doped TiO_2 Nanoparticle Based Visible Light Photocatalyst by Modified Peroxide Sol−Gel Method. *J. Phys. Chem. C* **2008**, *112* (37), 14595−14602.

(5) Tojo, S.; Tachikawa, T.; Fujitsuka, M.; Majima, T. Iodine-Doped TiO_2 Photocatalysts: Correlation Between Band Structure and Mechanism. *J. Phys. Chem. C* **2008**, *112* (38), 14948−14954.

(6) Gratzel, M. Photoelectrochemical Cells. *Nature* **2001**, *414* (6861), 338−344.

(7) Smeigh, A. L.; Katz, J. E.; Brunschwig, B. S.; Lewis, N. S.; McCusker, J. K. Effect of the Presence of Iodide on the Electron Injection Dynamics of Dye-Sensitized TiO_2-Based Solar Cells. *J. Phys. Chem. C* **2008**, *112* (32), 12065−12068.
(8) Greijer, H.; Lindgren, J.; Hagfeldt, A. Resonance Raman Scattering of a Dye-Sensitized Solar Cell: Mechanism of Thiocyanato Ligand Exchange. *J. Phys. Chem. B* **2001**, *105* (27), 6314−6320.
(9) Tian, H.; Yang, X.; Chen, R.; Zhang, R.; Hagfeldt, A.; Sun, L. Effect of Different Dye Baths and Dye-Structures on the Performance of Dye-Sensitized Solar Cells Based on Triphenylamine Dyes. *J. Phys. Chem. C* **2008**, *112* (29), 11023−11033.
(10) Tsuji, H.; Sakai, N.; Gotoh, Y.; Ishikawa, J. Photocatalytic Properties of Sol−Gel Titania Film Under Fluorescent-Light Irradiation Improved by Silver Negative-Ion Implantation. *Nucl. Instrum. Methods Phys. Res., Sect. B* **2006**, *242* (1−2), 129−132.
(11) Hu, C.; Lan, Y.; Qu, J.; Hu, X.; Wang, A. Ag/AgBr/TiO_2 Visible Light Photocatalyst for Destruction of Azodyes and Bacteria. *J. Phys. Chem. B* **2006**, *110* (9), 4066−4072.
(12) Lee, M. S.; Hong, S.-S.; Mohseni, M. Synthesis of Photocatalytic Nanosized TiO_2−Ag Particles with Sol−Gel Method Using Reduction Agent. *J. Mol. Catal. A: Chem.* **2005**, *242* (1−2), 135−140.
(13) Gorzkowska−Sobas, A.; Kusior, E.; Radecka, M.; Zakrzewska, K. Visible Photocurrent Response of TiO_2 Anode. *Surf. Sci.* **2006**, *600* (18), 3964−3970.
(14) Awazu, K.; Fujimaki, M.; Rockstuhl, C.; Tominaga, J.; Murakami, H.; Ohki, Y.; Yoshida, N.; Watanabe, T. A Plasmonic Photocatalyst Consisting of Silver Nanoparticles Embedded in Titanium Dioxide. *J. Am. Chem. Soc.* **2008**, *130* (5), 1676−1680.
(15) Hamal, D. B.; Klabunde, K. J. Synthesis, Characterization, and Visible Light Activity of New Nanoparticle Photocatalysts Based on Silver, Carbon, and Sulfur-Doped TiO_2. *J. Colloid Interface Sci.* **2007**, *311* (2), 514−522.
(16) Balan, L.; Malval, J. P.; Schneider, R.; Burget, D. Silver Nanoparticles: New Synthesis, Characterization and Photophysical Properties. *Mater. Chem. Phys.* **2007**, *104* (2−3), 417−421.
(17) Park, S. J.; Kim, S.; Lee, S.; Khim, Z. G.; Char, K.; Hyeon, T. Synthesis and Magnetic Studies of Uniform Iron Nanorods and Nanospheres. *J. Am. Chem. Soc.* **2000**, *122* (35), 8581−8582.
(18) Jana, N. R.; Pal, T. Redox Catalytic Property of Still-Growing and Final Palladium Particles: A Comparative Study. *Langmuir* **1999**, *15* (10), 3458−3463.
(19) Arabatzis, I. M.; Stergiopoulos, T.; Bernard, M. C.; Labou, D.; Neophytides, S. G.; Falaras, P. Silver-Modified Titanium Dioxide Thin Films for Efficient Photodegradation of Methyl Orange. *Appl. Catal. B: Environ.* **2003**, *42* (2), 187−201.
(20) Sclafani, A.; Mozzanega, M. N.; Pichat, P. Effect of Silver Deposits on the Photocatalytic Activity of Titanium Dioxide Samples for the Dehydrogenation or Oxidation of 2-Propanol. *J. Photochem. Photobiol., A* **1991**, *59* (2), 181−189.
(21) Stathatos, E.; Petrova, T.; Lianos, P. Study of the Efficiency of Visible-Light Photocatalytic Degradation of Basic Blue Adsorbed on Pure and Doped Mesoporous Titania Films. *Langmuir* **2001**, *17* (16), 5025−5030.
(22) Kawahara, K.; Suzuki, K.; Ohko, Y.; Tatsuma, T. Electron Transport in Silver-Semiconductor Nanocomposite Films Exhibiting Multicolor Photochromism. *Phys. Chem. Chem. Phys.* **2005**, *7* (22), 3851−5.
(23) Sung-Suh, H. M.; Choi, J. R.; Hah, H. J.; Koo, S. M.; Bae, Y. C. Comparison of Ag Deposition Effects on the Photocatalytic Activity of Nanoparticulate TiO_2 under Visible and UV Light Irradiation. *J. Photochem. Photobiol., A* **2004**, *163* (1−2), 37−44.
(24) Seery, M. K.; George, R.; Floris, P.; Pillai, S. C. Silver Doped Titanium Dioxide Nanomaterials for Enhanced Visible Light Photocatalysis. *J. Photochem. Photobiol., A* **2007**, *189* (2−3), 258−263.
(25) Es-Souni, M.; Es-Souni, M.; Habouti, S.; Pfeiffer, N.; Lahmar, A.; Dietze, M.; Solterbeck, C. H. Brookite Formation in TiO_2 Ag Nanocomposites and Visible-Light-Induced Templated Growth of Ag Nanostructures in TiO_2. *Adv. Funct. Mater.* **2010**, *20* (3), 377−385.
(26) Yang, L. B.; Jiang, X.; Ruan, W. D.; Yang, J. X.; Zhao, B.; Xu, W. Q.; Lombardi, J. R. Charge-Transfer-Induced Surface-Enhanced Raman Scattering on Ag−TiO_2 Nanocomposites. *J. Phys. Chem. C* **2009**, *113* (36), 16226−16231.
(27) Tanahashi, I.; Iwagishi, H.; Chang, G. Localized Surface Plasmon Resonance Sensing Properties of Photocatalytically Prepared Au/TiO_2 Films. *Mater. Lett.* **2008**, *62* (17−18), 2714−2716.
(28) Song, W.; Wang, Y. X.; Zhao, B. Surface-Enhanced Raman Scattering of 4-Mercaptopyridine on the Surface of TiO_2 Nanofibers Coated with Ag Nanoparticles. *J. Phys. Chem. C* **2007**, *111* (34), 12786−12791.
(29) Liu, Y. C.; Yu, C. C.; Hsu, T. C. Effect of TiO_2 Nanoparticles on the Improved Performances on Electrochemically Prepared Surface-Enhanced Raman Scattering-Active Silver Substrates. *J. Phys. Chem. C* **2008**, *112* (41), 16022−16027.
(30) Tanabe, I.; Matsubara, K.; Standridge, S. D.; Kazuma, E.; Kelly, K. L.; Sakai, N.; Tatsuma, T. Photocatalytic Growth and Plasmon Resonance-Assisted Photoelectrochemical Toppling of Upright Ag Nanoplates on a Nanoparticulate TiO_2 Film. *Chem. Commun.* **2009**, *24*, 3621.
(31) Matsubara, K.; Kelly, K. L.; Sakai, N.; Tatsuma, T. Plasmon Resonance-Based Photoelectrochemical Tailoring of Spectrum, Morphology and Orientation of Ag Nanoparticles on TiO_2 Single Crystals. *J. Mater. Chem.* **2009**, *19* (31), 5526.
(32) Armelao, L.; Barreca, D.; Bottaro, G.; Gasparotto, A.; Maccato, C.; Tondello, E.; Lebedev, O. I.; Turner, S.; Van Tendeloo, G.; Sada, C.; et al. Rational Design of Ag/TiO_2 Nanosystems by a Combined RF-Sputtering/Sol-Gel Approach. *ChemPhysChem* **2009**, *10* (18), 3249−3259.
(33) Hong, Z. C.; Perevedentseva, E.; Treschev, S.; Wang, J. B.; Cheng, C. L. Surface Enhanced Raman Scattering of Nano Diamond Using Visible-Light-Activated TiO_2 as a Catalyst to Photo-Reduce Nano-Structured Silver From $AgNO_3$ as SERS-Active Substrate. *J. Raman Spectrosc.* **2009**, *40* (8), 1016−1022.
(34) Kato, K.; Tsuzuki, A.; Torii, Y.; Taoda, H.; Kato, T.; Butsugan, Y. Morphology of Thin Anatase Coatings Prepared From Alkoxide Solutions Containing Organic Polymer, Affecting the Photocatalytic Decomposition of Aqueous Acetic Acid. *J. Mater. Sci.* **1995**, *30* (3), 837−841.
(35) Pradeep, J. A.; Agarwal, P. Determination of Thickness, Refractive Index, and Spectral Scattering of an Inhomogeneous Thin Film with Rough Interfaces. *J. Appl. Phys.* **2010**, *108* (4), 043515(9).
(36) Jin, R. Photoinduced Conversion of Silver Nanospheres to Nanoprisms. *Science* **2001**, *294* (5548), 1901−1903.
(37) Tada, H.; Tanaka, M. Dependence of TiO_2 Photocatalytic Activity upon Its Film Thickness. *Langmuir* **1997**, *13* (2), 360−364.
(38) Yu, J. G.; Zhao, X. J.; Zhao, Q. N. Effect of Film Thickness on the Grain Size and Photocatalytic Activity of the Sol-Gel Derived Nanometer TiO_2 Thin Films. *J. Mater. Sci. Lett.* **2000**, *19* (12), 1015−1017.
(39) Stiles, P. L.; Dieringer, J. A.; Shah, N. C.; Van Duyne, R. R. Surface-Enhanced Raman Spectroscopy. *Annu. Rev. Anal. Chem.* **2008**, *1*, 601−626.
(40) Lee, S. J.; Guan, Z. Q.; Xu, H. X.; Moskovits, M. Surface-Enhanced Raman Spectroscopy and Nanogeometry: The Plasmonic Origin of SERS. *J. Phys. Chem. C* **2007**, *111* (49), 17985−17988.
(41) Hering, K.; Cialla, D.; Ackermann, K.; Dorfer, T.; Moller, R.; Schneidewind, H.; Mattheis, R.; Fritzsche, W.; Rosch, P.; Popp, J. SERS: A Versatile Tool in Chemical and Biochemical Diagnostics. *Anal. Bioanal. Chem.* **2008**, *390* (1), 113−124.
(42) Wang, H.; Levin, C. S.; Halas, N. J. Nanosphere Arrays with Controlled Sub-10-nm Gaps as Surface-Enhanced Raman Spectroscopy Substrates. *J. Am. Chem. Soc.* **2005**, *127* (43), 14992−14993.
(43) Li, D.; Wu, S.; Wang, Q.; Wu, Y.; Peng, W.; Pan, L. Ag@C Core−Shell Colloidal Nanoparticles Prepared by the Hydrothermal Route and the Low Temperature Heating−Stirring Method and Their Application in Surface Enhanced Raman Scattering. *J. Phys. Chem. C* **2012**, *116* (22), 12283−12294.

(44) Li, L. L.; Fang, P. P.; Yang, Z. L.; Huang, E. D.; Wu, D. Y.; Ren, B.; Tian, Z. Q. Size Dependent SERS Activity of Gold Nanoparticles Studied by 3D-FDTD Simulation. *Spectrosc. Spect. Anal.* **2009**, *29* (5), 1222−1226.